Truncations and *in silico* Docking to Enhance the Analytical Response of Aptamer-Based Biosensors

*Minh-Dat Nguyen[a], Meghan T. Osborne[b], Guy Terence Prevot[a], Zachary R. Churcher[b], Philip E. Johnson[b], Lena Simine[c], Philippe Dauphin-Ducharme[a]**

[a]Département de chimie, Université de Sherbrooke, Sherbrooke, Québec J1K 2R1, Canada

[b]Department of Chemistry, York University, Toronto, Ontario M3J 1P3, Canada

[c]Department of Chemistry, McGill University, Montreal, Quebec H3A 0B8, Canada

Corresponding author.

Email: philippe.dauphin.ducharme@usherbrooke.ca

ABSTRACT

Aptamers are short oligonucleotides capable of binding specifically to various targets (i.e., small molecules, proteins, and whole cells) which have been introduced in biosensors such as in the electrochemical aptamer-based (E-AB) sensing platform. E-AB sensors are comprised of a redox-reporter-modified aptamer attached to an electrode that undergoes, upon target addition, a binding-induced change in electron transfer rates. To date, E-AB sensors have faced a limitation in the translatability of aptamers into the sensing platform presumably because sequences obtained from Systematic Evolution of Ligands by Exponential Enrichment (SELEX) are typically long (> 80 nucleotides) and that obtaining structural information remains time and resource consuming. In response, we explore the utility of aptamer base truncations and *in silico* docking to improve their translatability into E-AB sensors. Here, we first apply this to the glucose aptamer, which we characterize in solution using NMR methods to guide design and translate truncated variants in E-AB biosensors. We further investigated applicability of the truncation and computational approaches to five other aptamer systems (vancomycin, cocaine, methotrexate, theophylline, and ochratoxin A) from which we derived functional E-AB sensors. We foresee that our strategy will increase the success rate of translating aptamers into sensing platforms to afford low-cost measurements of molecules directly in undiluted complex matrices.

KEYWORDS

Aptamer docking, Aptamer truncations, Electrochemical aptamer-based biosensors, glucose biosensor, Electrochemical impedance spectroscopy, NMR spectroscopy.

INTRODUCTION

Aptamers are short oligonucleotides obtained via "Systematic Evolution of Ligands by Exponential Enrichment" (SELEX) that are capable of binding with high specificity to a wide variety of targets (*e.g.*, small molecules, proteins, and whole cells).[1–3,4] Due to their target-recognition capabilities, stability and ease of modification, aptamers have increasingly been utilized in several biosensing platforms to enable development of new point-of-need biomedical tools.[4,5]

Electrochemical aptamer-based (E-AB) biosensors are an example of such a platform. E-AB biosensors are comprised of a redox-reporter-modified aptamer that is electrode-bound, which upon aptamer target addition undergoes a change in electron transfer rate[6]. Such change can be directly measured using different electroanalytical techniques to quantitively report on the target concentration to support direct, reagent-less, and real-time molecular measurements in different undiluted biological matrices.[7–10]

To date, while several E-AB biosensors have been developed for different molecules[8,9,11–14], a major limitation that hampers their widespread use remains the translation of aptamers into the sensing platform.[12] We presume that this is because: 1) aptamers obtained via SELEX are often long (typically ~60-80-mer)[15], which may place the ligand binding site far from the electrode surface minimizing measurable changes in electron transfer rates; and 2) only a handful of aptamers (e.g., cocaine[16]-, adenosine triphosphate[17]-, ochratoxin[18]-, thrombin[19]-binding aptamers) have been structurally characterized using nuclear magnetic resonance spectroscopy[18,20,21] and X-ray crystallography[22–24]. As a result, it remains challenging to identify the ligand binding site to reengineer new aptamer sequences to maximize binding-induced changes in E-AB sensors.[25–29]

Only a small fraction of the total number of nucleotides in an aptamer sequence is involved in target recognition.[20,21,30–34] Fifteen of the 60 nucleotides composing the α-thrombin parent aptamer, for example, are responsible for binding.[35,36] Considering that E-AB sensors rely on changes in electron transfer rates of the redox reporter that occur within short distances (< 1-2 nm)[37–39] from the electrode, shortening sequences could improve their analytical responses.[8,27] To guide aptamer length reduction, a few groups use isothermal calorimetry titrations (ITC) and circular dichroism (CD)[14,26,40,41] to gain information on aptamer function such as binding and conformational changes. ITC and CD, however, can report on changes that occur far from aptamer tagging positions which would not support strong E-AB sensor signaling.[26,41] Xiao and co-workers, in contrast, elegantly provided an experimentally guided approach to yield functioning E-AB sensors for adenosine or fentanyl-binding aptamers.[42–44] For this, the authors produce shorter aptamer variants by inhibiting exonucleases digestion when an aptamer is in the presence of target. This approach has shown great promise to obtaining an ideally optimized aptamer.[42]

To engineer aptamers into their shortest sequences for E-AB sensors we decided to perform truncations (removing nucleotides from the 3' and 5' extremities of the aptamer) of aptamers and investigate the applicability of *in silico* docking computational tools that do not require advanced programming skills. We first studied the glucose[45] aptamer through NMR spectroscopy to enable the design of a functional E-AB sensor through base truncations. Concomitantly, we performed *in silico* docking and corroborated potential nucleotides involved in target binding identified via NMR spectroscopy. Motivated by these results, we truncated four other DNA aptamers binding low-molecular-weight targets including methotrexate[40], theophylline[46], cocaine[21], and vancomycin[7]. In doing so, we observed that for all truncated variants in which we brought the predicted (as per docking) binding region closer to the electrode improved the response of E-AB

sensors. We thus envision that performing truncations and ligand docking could provide for rapid translation of aptamers in different sensing technologies.

RESULTS AND DISCUSSION

As a test bed for our study, we decided to use the glucose binding aptamer previously reported by Nakatsuka and co-workers[45]. Given that its target binding region and structure has still not been studied in great lengths, we first set out to characterize it with NMR spectroscopy. The 1D ^{1}H NMR spectrum of the free parent glucose aptamer (**Figure 1A**) revealed ~ 7 peaks in the Watson-Crick region of its imino ^{1}H spectrum indicating base pairing that we confirmed with a 2D NOESY experiment (**Figure S1**). These assignments confirmed the presence of two stems separated by a large asymmetrical bulge region (**Figure 1B**). The addition of glucose results in the formation of many new imino peaks (**Figure 1A**) and specifically ones from nucleotides in the bulge region indicated the likely formation of new base pairs (G11-G27, G9-C32 and T8-A33) supporting ligand-induced structure formation (**Figure 1B**).

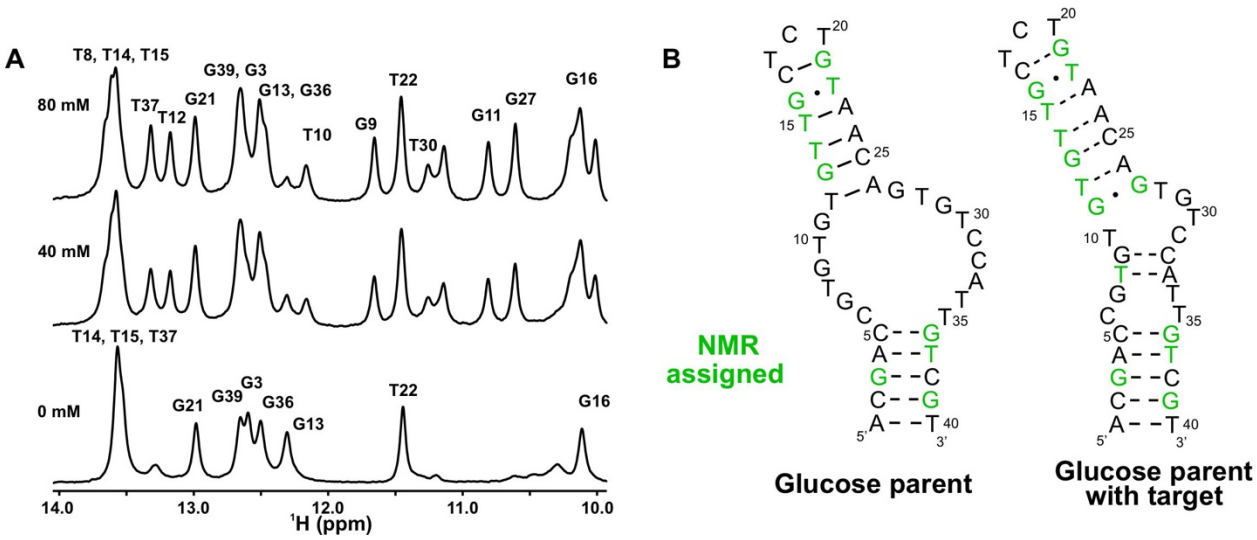

Figure 1. In performing (**A**) 1D ^{1}H NMR and 2D NOESY experiments (see **Figure S1**), we were able to assign nucleotide imino ^{1}H signals of the glucose parent aptamer as highlighted in green in the predicted secondary structure in (**B**). Increasing the glucose concentration results in structure formation and new imino proton signals to appear (see 1D ^{1}H NMR in (**A**) and in 2D NOESY in **Figure S1**)). From these results, glucose appears to bind in the bulge region of the parent aptamer. NMR spectra acquired at 0.5-1.5 mM in 250 mM NaCl, 10 mM $H_xNa_yPO_4$, pH 7.6, 10% $^{2}H_2O$/90% $^{1}H_2O$ at 5 ˚C.

Having assigned imino protons of nucleotides in the glucose aptamer, we were interested to gain further insights into the location of ligand binding. For this, we studied different mutations of the parent aptamer (**Figure 2**). When changing nucleotides in the bulge region of the aptamer (Glu-mod1, Glu-mod2, Glu-mod3, Glu-mod4, Glu-mod5, Glu-mod6, Glu-mod9 and Glu-mod10), we observed no discernable change in the NMR spectrum when adding target, indicating that these variants were unable to bind glucose (as an example see **Figure S2A** for Glu-mod1). When mutations were performed outside of the bulge region (Glu-mod7 and Glu-mod8), in contrast, we still observed changes in the NMR spectrum indicative of aptamer binding (**Figures S2B** and **C**). These observations indicate that glucose likely interacts with nucleotides found in the bulge to result in ligand binding.

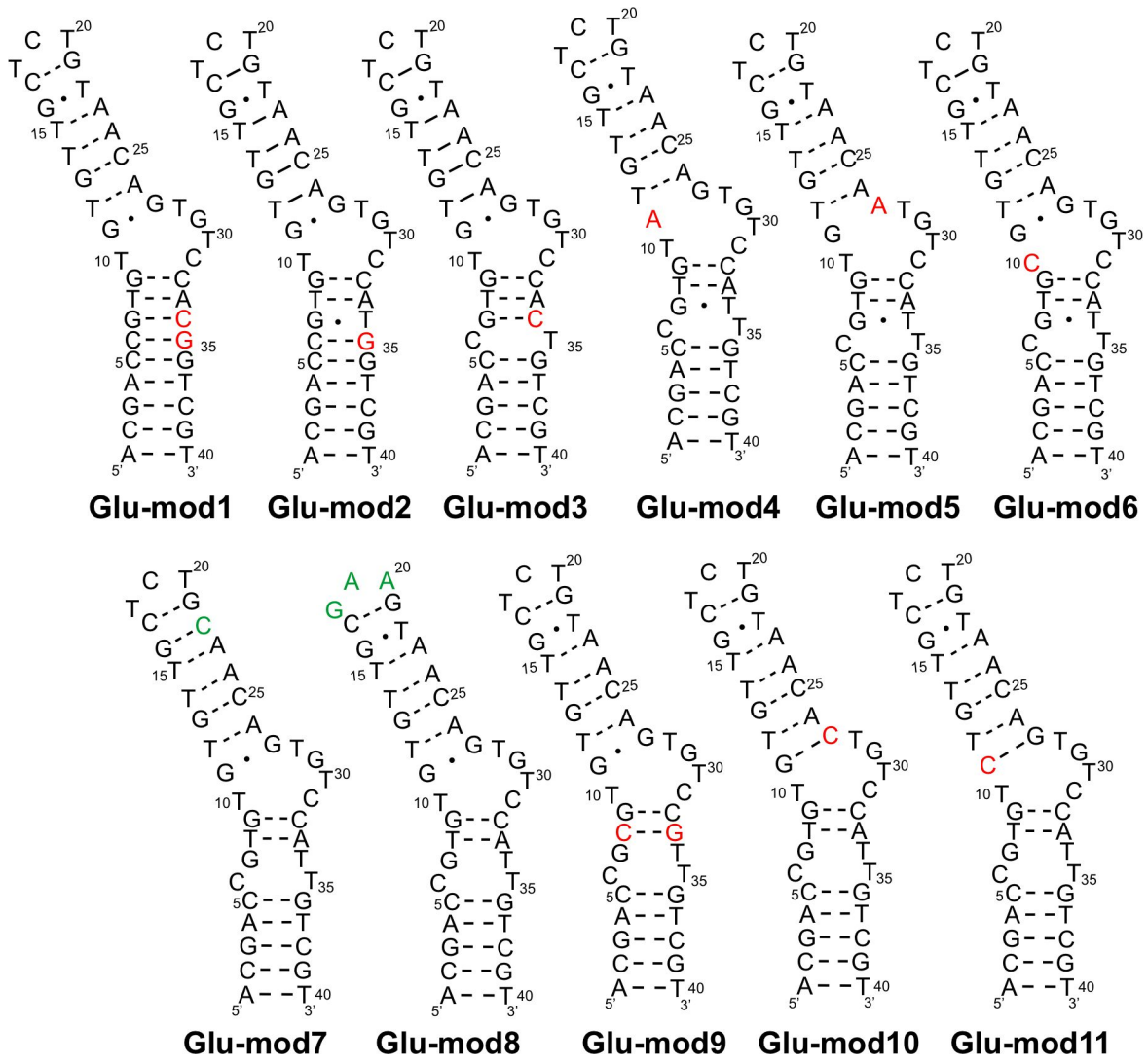

Figure 2. Predicted secondary structures of the different sequence variants of the glucose parent aptamer we tested via point mutations to determine the ligand binding region. Nucleotides in red are ones that inhibited glucose binding while ones in green did not alter target binding.

Guided by these results, we designed truncated variants of the glucose aptamer to produce a functional E-AB sensor. We envision that performing truncations increases the aptamer flexibility and brings the identified binding site closer to the electrode surface allowing for an enhancement in E-AB sensor response.[47] We produced 2 truncated variants of the glucose aptamer by removing three and six terminal base pairs from the parent aptamer (**Figure 3A**). Along with the parent aptamer, we functionalized the 3' and 5' extremities of each variant with a methylene

blue redox reporter and a thiol anchor. We fabricated E-AB sensors using known procedures[48] with the modified sequences and interrogated each using electrochemical impedance spectroscopy due to its ability to deconvolute the different electrochemical processes occurring at different time scales and maximize E-AB sensors' faradaic contribution to the measured current. This involved fixing a sinusoidally oscillating potential at methylene blue's reduction potential and measuring the alternating current response. We then fitted the impedimetric responses to a known equivalent circuit composed of 4 elements (i.e., solution resistance (R_{sol}), electrical double-layer formation (C_{int}), charge transfer resistance (R_{CT}) and the redox reporter pseudocapacitance (C_{DNA})).[49] We observed that R_{sol}, C_{int} and C_{DNA} remained constant as a function of target concentration while R_{CT} varied (**Figure S3**). The parent glucose aptamer and its 6-trunc variant showed no electrochemical change upon addition of target. The 3-trunc variant, in contrast, showed the largest response (**Figure 4A**). These results suggest that T35 of the aptamer, as seen in our NMR spectroscopy mutation study, participate in binding with glucose.

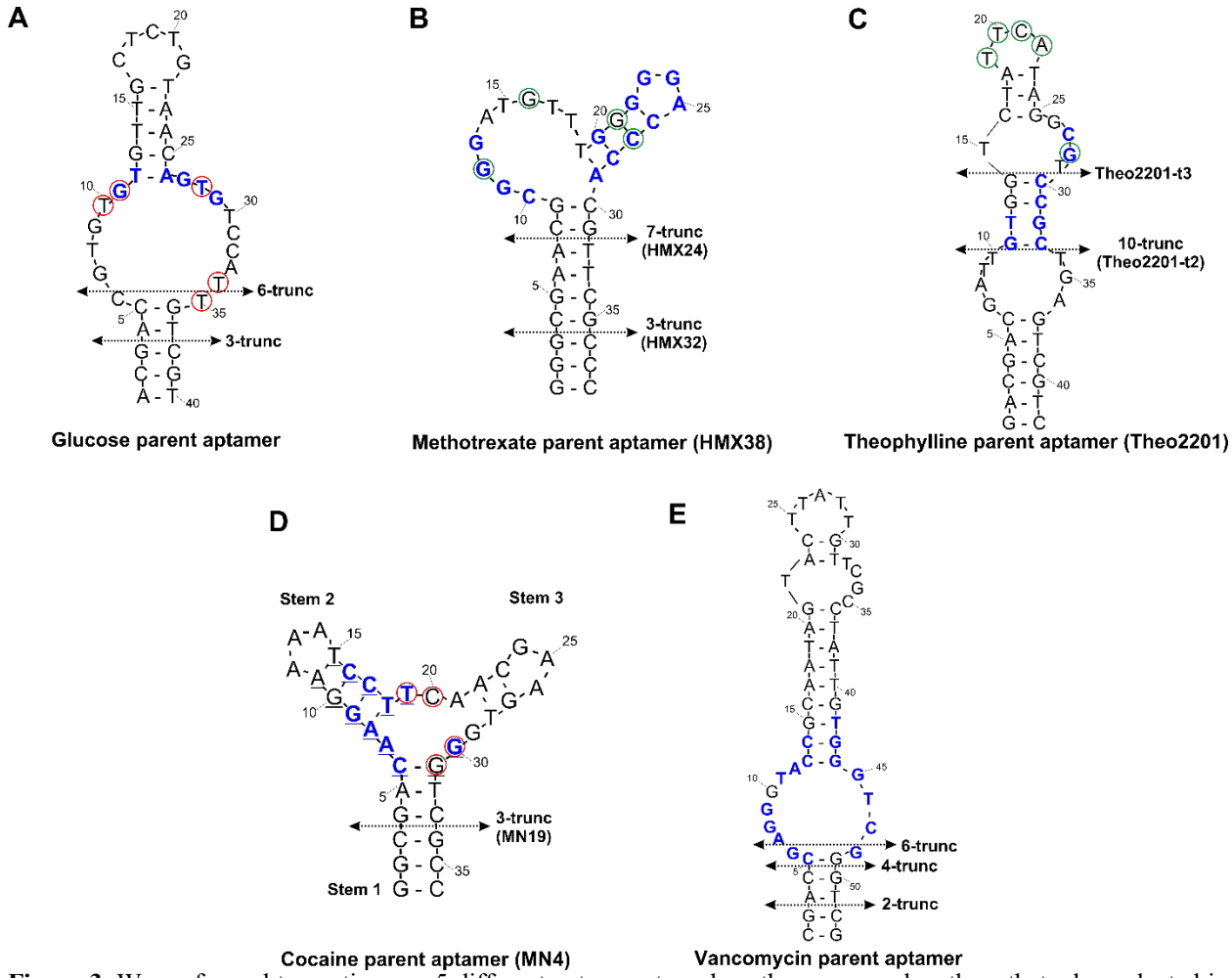

Figure 3. We performed truncations on 5 different aptamers to reduce the sequence length so that when adapted in the E-AB sensing platform this would position the ligand binding site closer to the electrode. The dashed lines on each aptamer show the different nucleotides we discarded. The blue residues indicate the interacting nucleotides predicted by *in silico* docking of the top-ranking docked target conformation with the corresponding aptamer binding **(A)** glucose, **(B)** methotrexate, **(C)** theophylline, **(D)** cocaine and **(E)** vancomycin. For MN4 and glucose parent aptamers, the nucleotides circled in red represent ones experimentally identified in binding from NOEs or where mutations impede binding in NMR studies. The nucleotides circled in green are ones experimentally identified where mutations impede target binding as per ITC method as identified previously in past reports.

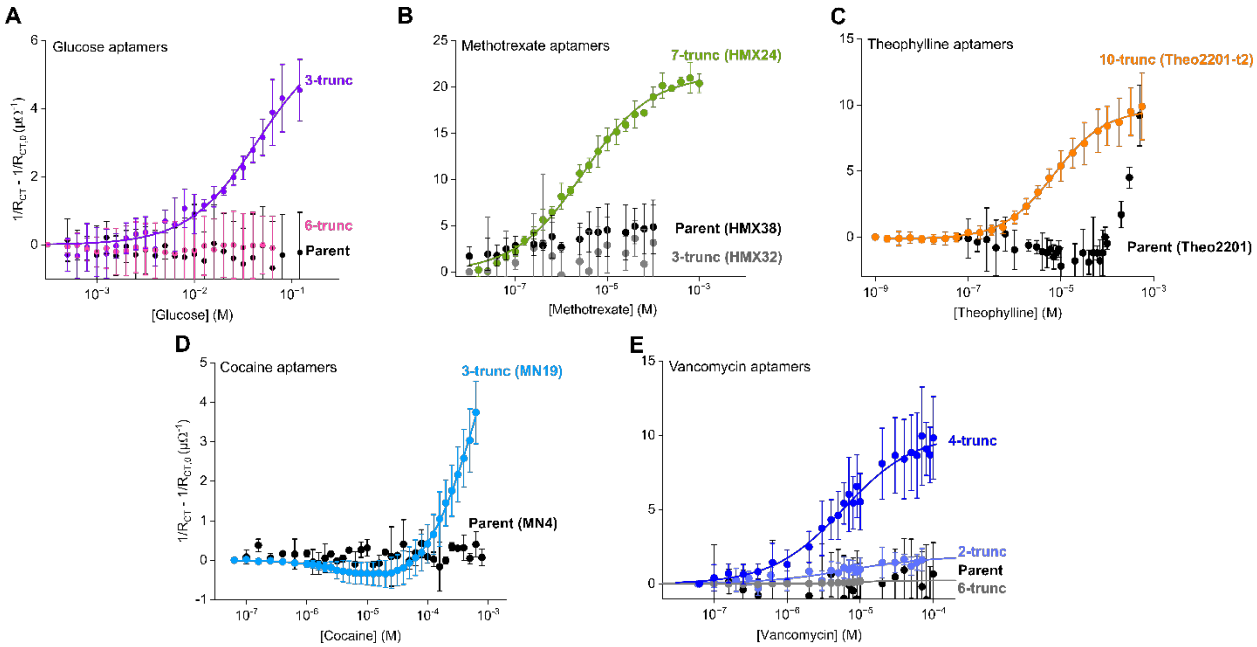

Figure 4. Aside from variants in which we removed identified binding nucleotides, all E-AB sensors for **(A)** glucose, **(B)** methotrexate, **(C)** theophylline, **(D)** cocaine and **(E)** vancomycin designed using truncated aptamers produced increased responses when challenged with their corresponding targets. We show this by modifying the 3' and 5' termini of all aptamers with a methylene blue redox reporter and a thiol anchor from which we fabricated E-AB sensors. We then acquired electrochemical impedance spectroscopy results that we fitted using an equivalent circuit diagram to quantify changes associated with interfacial charge transfer resistances (R_{CT}). We derived from these fits the dissociation constant (see K_D values in **Table 1**). The errors illustrate the standard deviation of signals produced by at least three sensors independently fabricated and tested. In certain cases, we did not obtain sensor saturation as we typically refrain from reaching high target concentrations due to changes in pH or non-specific interaction with the aptamer ultimately resulting in confounding effects of E-AB sensors.[50] Each aptamer was tested in different buffers (see supporting information for more details) to match with the SELEX conditions used.

Table 1. We report here the measured limits of detection and K_D values obtained using electrochemical impedance spectroscopy (EIS) that we compare to isothermal titration calorimetry (ITC) or nuclear magnetic resonance (NMR) results previously reported.

Target	Aptamer	Limit of detection (μM)	K_D value (μM)	
			EIS	ITC/NMR
Glucose	Parent	-	n/a	5000 ± 2000
	3-trunc	7900	40000 ± 10000	> 10000
	6-trunc	-	n/a	-
Methotrexate	Parent (HMX38)	-	n/a	0.165 ± 0.083 [40]
	3-trunc (HMX32)	-	n/a	0.488 ± 0.234 [40]
	7-trunc (HMX24)	0.04	2.9 ± 0.3	0.529 ± 0.153 [40]
Theophylline	Parent (Theo2201)	-	n/a	0.51 ± 0.13 [46]
	10-trunc (Theo2201-t2)	0.25	7.1 ± 0.5	9.8 [46]
Cocaine	Parent (MN4)	-	n/a	8.6 ± 4.4 [51]
	3-trunc (MN19)	0.63	6.3 ± 0.8 *	17 ± 3 [51]

Vancomycin	Parent	-	n/a	0.14 ± 0.02 [41]
	2-trunc	-	7 ± 5	n/a
	4-trunc	0.63	5.9 ± 0.7	52 ± 20 [41]
	6-trunc	-	n/a	n/a

n/a: there is no concentration-dependent signal. * K_D value for the high affinity binding site.

Given that E-AB sensors response can be complicated by several parameters especially when at high target concentrations,[50] we wanted to confirm that the response of our E-AB glucose 3-trunc variant is ascribed to target binding. For this we performed solution-based characterization in NMR by monitoring the increase of 6 imino proton peak intensities as glucose was added, a reliable approach due to the weak affinity of this aptamer (**Figure S4** and **Table S4**). When looking at the parent variant, we determined an average K_D value of 5 ± 2 mM closely matching with that measured by fluorescence[45] and 2-aminopurine methods[52]. As was previously observed by Lu and co-workers[52], this binding appears specific since when we added galactose, an epimer of glucose, we observed no chemical shift changes or new imino signal appearance indicating that no detectible binding occurs under these conditions (**Figure S2D**). We likewise determined the affinity of the Glu-mod7 and Glu-mod8 variants (mutations in the upper stem portion of the aptamer) and found those to have K_D values of 2.9 ± 0.3 and 12 ± 3 mM, respectively, closely approaching our results for the parent variant. When characterizing our glucose 3-trunc variant, we also observed binding with NMR methods, albeit at higher concentrations, with an affinity comparable to when adapted into the E-AB sensing platform (unsaturated titration even with 80 mM of glucose added in comparison to a K_D value of 40 ± 10 mM when in E-AB sensors) (**Figure S2E**). Together, these observations further support that glucose binds in the bulge region of the aptamer.

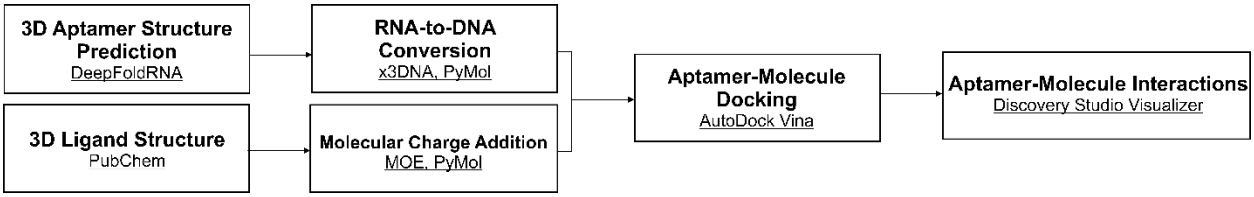

Figure 5. The computational workflow to predict an aptamer tertiary structure and nucleotides involved in target binding consists of four steps. We start by predicting the aptamer tertiary structure using the online bioinformatic tool DeepFoldRNA[53] using the aptamers' sequences in their RNA format. Next, we modified the predicted RNA aptamer structure by converting uracil residues to thymines using another web-based tool, x3DNA[54], followed by removal of the 2'-OH groups of the RNA structures using PyMol[55] to obtain a rough DNA aptamer model. Target structures provided by PubChem and target charges are calculated using a molecular operating environment (MOE).[56] Third, we performed blind aptamer-target docking via AutoDock Vina.[57] Finally, out of the 9 possible ligand conformations obtained, we analyzed the top candidate using Discovery Studio Visualizer,[58] to determine an estimation of aptamer-ligand interactions and nucleotides involved in binding.

To support our experimental identification of the ligand binding site in aptamers, we explored the use of conventional computational *in silico* docking tools (**Figure 5**). With these tools, we do not aim at precisely predicting the tertiary structure of aptamers as current tools do not provide accurate representations, especially of non-Watson-Crick base pairs prevalent in DNA aptamers. Further experimental validation of the tertiary structure should be provided via, for example, ^{13}C and ^{15}N labelling in NMR, X-Ray or cryo-EM. We set out to test conventional computational tools by generating a 3-D model for the aptamer's tertiary structure using DeepFoldRNA[53]. DeepFoldRNA is a web-based software that models tertiary structures using deep learning techniques, which has shown improved performances on benchmark datasets like Rfam families or RNA-Puzzle experiments with root mean square deviation (RMSD) averages of 2.69 Å in comparison to other models. To use DeepFoldRNA, as others have prior to us,[59–63] we transposed the glucose aptamer sequence into RNA format. From the 10 predictions generated by the algorithm, we picked the one with the lowest RMSD and then swapped the uracils for thymines in the structure using the web-based tool, x3DNA,[54] prior to removing the 2'-OH on the ribose backbone using PyMol.[55] Next, we performed blind docking of the target molecules to the

predicted aptamer structures[64] using AutoDock Vina (version 1.2.0)[57], a widely used open-source molecular docking software program. This tool has successfully performed virtual screening of small molecules binding to macromolecular receptors such as proteins.[65–68] We modified the grid box dimensions that was generated by AutoDock Vina to cover all possible interactions between the aptamer and its target (**Table S5**). Following docking we obtained up to nine binding target poses that we classify per increasing Vina score (in kcal mol^{-1}) and RMSD (**Table S6**). The former parameter is an equilibrium state that reflects the aptamer-target complex stability while the later informs on the changes in the conformation of the target compared to the model of best affinity.[69] The predicted structures were clustered with a 2 Å RMSD cutoff that we used as a criterion to predict the bound structure.[70–72] We therefore chose the best-scoring binding pose having the lowest energy value and the best alignment that has 0 RMSD.[25,57,73–75]

Conventional *in silico* docking computational results to determine the ligand binding site of the glucose aptamer appear to agree with our NMR spectroscopy-derived observations. We observed this through a final computational analysis step involving visualization of the ligand binding site and identification of the aptamer-ligand interactions using Discovery Studio Visualizer, part of the suite of software developed and distributed by Dassault Systems BIOVIA.[76] This software allowed us to identify the interactions such as hydrogen bonds, Van der Waals, halogen binding, π-π stacking, etc[4,5,77] in the docked target-aptamer complexes (**Figure S5**). When visualizing interactions of the glucose-binding aptamer docked structure, we observed that the target inserted into the bulge and interacted with 6 (G11, T12, A26, G27, T28, and G29 in **Figure 3D**) of the 40 nucleotides in the glucose sequence, 2 (G11 and G27 in **Figure 3D**) of which identified as inhibiting binding via NMR spectroscopy. We foresee that the loss of response of the 6-trunc variant in buffer attest that T34 and T35 are needed for target binding either by interacting

with the ligand or stabilizing the structure necessary for binding as indicated by our NMR results. Together these results illustrate that docking tools currently available could provide for a rapid entry-point to assess the ligand binding site of the aptamer.

Encouraged by the successful translation of the glucose aptamer into an E-AB sensor, we proceeded to derive truncated variants of 4 other aptamers binding small molecule ligands (methotrexate[40], theophylline[46], cocaine[21], and vancomycin[7]). We shortened the methotrexate-binding aptamer (HMX38) by removing 3 and 7 base pairs to generate two truncated variants (3-trunc and 7-trunc) (**Figure 3B**). For the theophylline-binding aptamer, we decided to fully remove the stem and loop regions below G11 and C33 of the Theo2201 aptamer to produce the 10-trunc variant (also known as Theo2201-t2) (**Figure 3C**). With the cocaine-binding aptamer, we removed three base pairs from its extremities to produce the variant we refer as MN19 (**Figure 3D**). Finally, we decided to produce 3 truncated variants of the vancomycin aptamer (2-trunc, 4-trunc, and 6-trunc) (**Figures 3E**). Similar to the glucose aptamer, we functionalized the 3' and 5' extremities of each parent aptamer and its variants with a methylene blue redox reporter and a thiol anchor so that we could use each as an E-AB sensor.

Truncating the methotrexate, theophylline, cocaine, and vancomycin aptamers resulted in an increased E-AB sensor response. We showed this by fabricating E-AB sensors from the parent and truncated variants of these aptamers (**Figure 4**). By exposing methotrexate E-AB sensors to increasing amounts of target, we found that the parent and 3-trunc aptamers did not exhibit any target-induced response while the 7-trunc aptamer showed sigmoidal responses (**Figure 4B** and **Table 1**). Similarly, the theophylline E-AB sensors fabricated from a 10-trunc variant also produced larger response in comparison to the parent aptamer which did not return any response at low target concentrations (**Figure 4C** and **Table 1**). When challenging the MN4 parent aptamer

and the corresponding MN19 truncated variant with increasing amounts of cocaine, only the 3-trunc MN19 variant showed a measurable response (**Figure 4D** and **Table 1**). For the vancomycin aptamer truncated variants, we measured the largest maximal signal change for the 4-trunc variant. The 6-trunc variant of this aptamer, however, did not show any response when exposed to increasing amounts of vancomycin (**Figure 4E** and **Table 1**).

We again observe agreement between our computational results and ones obtained experimentally for the other aptamers. In looking at the methotrexate, theophylline, cocaine and vancomycin aptamers, nucleotides identified via docking closely match ones reported to be important to maintain binding in previous ITC and NMR mutation studies (see supporting information for more details). For instance, docking of methotrexate to its aptamer showed that binding occurred in the loop (C10, G11, G12, G13) and the stem-loop (G20, G22, G23, G24, A25, C26, C27, C28, A29) (**Figures 3B** and **S6**) consistent with the study of He and co-workers.[40] For the theophylline aptamer, docking predicted the binding site to be located at G11, T12, C27, G28, C30, C31, G32, and C33 of the aptamer (**Figures 3C** and **S7**), in line with Huang and colleagues[46] who found that only when the second stem (above T15 and T29) was removed did binding was abolished. When visualizing interactions of the MN4 cocaine-binding aptamer docked structure, we observed that the target inserted into the core of a three-way junction structure and interacted with 9 out of the 36 nucleotides in the MN4 sequence (C6, A7, A8, G9, C16, C17, T18, T19 and G30) (**Figures 3D** and **S8**). Of these, two nucleotides (T19 and G30) match those previously identified as making nuclear Overhauser effect (NOE) contacts with the aromatic ring of cocaine. While docking did not find two other nucleotides (C20 and G31) previously identified as making NOE contacts with cocaine, these were neighboring nucleotides to ones identified by docking (T19 and G30). Other nucleotides that docking identifies as potentially interacting with cocaine and not

identified by NOE interactions (C6, A7, A8, G9, C16, C17, T18) are at or adjacent to the junction and can plausibly interact with cocaine. In our previous study[16] we just reported NOE interaction to the aromatic group on cocaine limiting the reported nucleotides to a subset of those interacting with the ligand. Additionally, some of the nucleotides identified by docking may also reflect the identity of nucleotides at a lower affinity binding site previously identified at low NaCl concentrations.[21] Finally, blind docking showed that the vancomycin was predicted to bind to its aptamer at C5, G6, A7, G8, G9, T11, A12, C13, C14, T42, G43, G44, G45, T46, C47, and G48 (**Figures 3E** and **S9**) in agreement with ITC results of Shaver and co-workers.[41] In accordance with our sensor results, G6 appears as essential to support binding in this E-AB sensor and its removal decreases the measured response. This latter example illustrates the ability of the computational tools to predict which nucleotides are essential in binding with target and thus could help guide the design of E-AB sensors.

All truncated aptamer variants that did not affect the ligand binding site determined computationally or via NMR spectroscopy exhibited improved E-AB sensor response in comparison to the longer parent sequences. We presume that the increase in sensor response is because of two intertwined phenomena. Specifically, when looking at the cocaine-binding aptamer, by truncating MN4, we destabilize the conformation of the aptamer[21,26,78] which increases the probability with which the redox reporter competes with the ligand-binding site.[79] Indeed, we find lower electron transfer rates when the truncated MN19 sensors are in absence of target (**Figures S11A-B**). The addition of target brings the redox reporter closer to the electrode or changes its reorganizational energy sufficiently to result in larger differences in electron transfer rates with the unbound configuration.[27,47] The observation of such destabilization appears to also hold in cases of other aptamer systems (**Figures S10** and **S11**) which could suggest for similarities

in signaling mechanism. Second, by truncating the aptamer, the identified ligand and redox reporter binding site is brought closer to the electrode surface.[80] Given the exponential dependence of the tunneling current, which is thought to be the main electron transfer mechanism involved in these systems,[81] reducing this distance allows us to increase our resolution with which we are able to resolve the redox-reporter competition mechanism. Thus, we envision that aptamer truncations represent a necessary post-SELEX procedure to translate aptamers into functional E-AB biosensors.

CONCLUSION

In this study, we explore the use of truncations and computational docking to predict the location of the aptamer-ligand binding site to accelerate sequence design and in turn fabricate functional E-AB biosensors. Doing so, we found that, in comparison to parent aptamers, all truncated variants exhibited improved responses with some responding in clinically relevant ranges. We presume that the improved analytical performances originated from an increased change in aptamer flexibility between the free and bound states and a proximal binding site to the electrode surface.[27,47] While predicting aptamer tertiary structures and identifying all the nucleotides involved in target binding with any certainty poses as a challenge, the computational docking simulation outlined here appears to provide useful insights into the target binding region to allow for aptamer engineering. We foresee that the development of more accurate structure prediction tools and studies incorporating molecular dynamics simulations could help us further refine results obtained from docking, confirm the predicted binding mode and provide an estimate of the binding energy.[82–84] This will ultimately, we envision, accelerate the development of new aptamer-based

sensors able to measure molecules of interest for different uses directly in undiluted complex matrices.

AUTHOR INFORMATION

Corresponding Author

Email: philippe.dauphin.ducharme@usherbrooke.ca

Notes

Authors declare no conflict of interest related to this research.

Author Contributions

M.-D.N. designed, performed all docking studies, and interpreted results. G.T.P. performed all EIS measurements and helped M.-D.N. to prepare some of the docked aptamer-target complex figures. M.T.O. and Z.R.C. performed all characterization of the glucose aptamer in solution using NMR spectroscopy. M.-D.N. designed the research project and wrote the manuscript jointly with P.D.D., P. E. J. and L. S.

Supporting Information Available:

Docking results and predicted structures for all aptamers, experimental methods for E-AB biosensors fabrication and characterization, E-AB biosensors impedimetric results and NMR characterization of glucose aptamer with its variants. The molecular docking results of this study are available from the corresponding author upon reasonable request.

ACKNOWLEDGMENTS

The authors would like to acknowledge the Fonds de Recherche du Québec – Nature et Technologies and Natural Sciences and Engineering Research Council of Canada for funding this project via the NOVA Grant program. Special thanks to Dr. Kien Tran, Institut de recherche en immunologie et en cancérologie de l'Université de Montréal for insightful discussions on small-molecule docking. We also thank Yunus Kaiyum (York University) for help in preparing some of the figures involving the NMR data.

REFERENCES

(1) Jayasena, S. D. Aptamers: An Emerging Class of Molecules That Rival Antibodies in Diagnostics. *Clin. Chem.* **1999**, *45* (9), 1628–1650. https://doi.org/10.1093/clinchem/45.9.1628.

(2) Cruz-Toledo, J.; McKeague, M.; Zhang, X.; Giamberardino, A.; McConnell, E.; Francis, T.; DeRosa, M. C.; Dumontier, M. Aptamer Base: A Collaborative Knowledge Base to Describe Aptamers and SELEX Experiments. *Database* **2012**, *2012*, bas006–bas006. https://doi.org/10.1093/database/bas006.

(3) DeRosa, M. C.; Lin, A.; Mallikaratchy, P.; McConnell, E. M.; McKeague, M.; Patel, R.; Shigdar, S. In Vitro Selection of Aptamers and Their Applications. *Nat. Rev. Methods Primers* **2023**, *3* (1), 54. https://doi.org/10.1038/s43586-023-00238-7.

(4) Bouchard, P. R.; Hutabarat, R. M.; Thompson, K. M. Discovery and Development of Therapeutic Aptamers. *Annu. Rev. Pharmacol. Toxicol.* **2010**, *50*, 237–257. https://doi.org/10.1146/annurev.pharmtox.010909.105547.

(5) Keefe, A. D.; Pai, S.; Ellington, A. Aptamers as Therapeutics. *Nat. Rev. Drug Discovery* **2010**, *9* (7), 537–550. https://doi.org/10.1038/nrd3141.

(6) Lubin, A. A.; Plaxco, K. W. Folding-Based Electrochemical Biosensors: The Case for Responsive Nucleic Acid Architectures. *Acc. Chem. Res.* **2010**, *43* (4), 496–505. https://doi.org/10.1021/ar900165x.

(7) Dauphin-Ducharme, P.; Yang, K.; Arroyo-Currás, N.; Ploense, K. L.; Zhang, Y.; Gerson, J.; Kurnik, M.; Kippin, T. E.; Stojanovic, M. N.; Plaxco, K. W. Electrochemical Aptamer-Based Sensors for Improved Therapeutic Drug Monitoring and High-Precision, Feedback-Controlled Drug Delivery. *ACS Sens.* **2019**, *4* (10), 2832–2837. https://doi.org/10.1021/acssensors.9b01616.

(8) Idili, A.; Arroyo-Currás, N.; Ploense, K. L.; Csordas, A. T.; Kuwahara, M.; Kippin, T. E.; Plaxco, K. W. Seconds-Resolved Pharmacokinetic Measurements of the Chemotherapeutic Irinotecan in Situ in the Living Body. *Chem. Sci.* **2019**, *10* (35), 8164–8170. https://doi.org/10.1039/C9SC01495K.

(9) Arroyo-Currás, N.; Somerson, J.; Vieira, P. A.; Ploense, K. L.; Kippin, T. E.; Plaxco, K. W. Real-Time Measurement of Small Molecules Directly in Awake, Ambulatory Animals. *Proc. Natl. Acad. Sci.* **2017**, *114* (4), 645–650. https://doi.org/10.1073/pnas.1613458114.

(10) Hou, H.; Jin, Y.; Wei, H.; Ji, W.; Xue, Y.; Hu, J.; Zhang, M.; Jiang, Y.; Mao, L. A Generalizable and Noncovalent Strategy for Interfacing Aptamers with a Microelectrode for the Selective Sensing of Neurotransmitters in Vivo. *Angew. Chem., Int. Ed.* **2020**, *59* (43), 18996–19000. https://doi.org/10.1002/anie.202008284.

(11) Ferguson, B. S.; Hoggarth, D. A.; Maliniak, D.; Ploense, K.; White, R. J.; Woodward, N.; Hsieh, K.; Bonham, A. J.; Eisenstein, M.; Kippin, T. E.; Plaxco, K. W.; Soh, H. T. Real-Time, Aptamer-Based Tracking of Circulating Therapeutic Agents in Living Animals. *Sci. Transl. Med.* **2013**, *5* (213), 213ra165-213ra165. https://doi.org/10.1126/scitranslmed.3007095.

(12) Arroyo-Currás, N.; Dauphin-Ducharme, P.; Scida, K.; Chávez, J. L. From the Beaker to the Body: Translational Challenges for Electrochemical, Aptamer-Based Sensors. *Anal. Methods* **2020**, *12* (10), 1288–1310. https://doi.org/10.1039/D0AY00026D.

(13) Schoukroun-Barnes, L. R.; Macazo, F. C.; Gutierrez, B.; Lottermoser, J.; Liu, J.; White, R. J. Reagentless, Structure-Switching, Electrochemical Aptamer-Based Sensors. *Annu. Rev. Anal. Chem.* **2016**, *9* (1), 163–181. https://doi.org/10.1146/annurev-anchem-071015-041446.

(14) Liu, Y.; Canoura, J.; Alkhamis, O.; Xiao, Y. Immobilization Strategies for Enhancing Sensitivity of Electrochemical Aptamer-Based Sensors. *ACS Appl. Mater. Interfaces* **2021**, *13* (8), 9491–9499. https://doi.org/10.1021/acsami.0c20707.

(15) Zhuo, Z.; Yu, Y.; Wang, M.; Li, J.; Zhang, Z.; Liu, J.; Wu, X.; Lu, A.; Zhang, G.; Zhang, B. Recent Advances in SELEX Technology and Aptamer Applications in Biomedicine. *Int. J. Mol. Sci.* **2017**, *18* (10), 2142. https://doi.org/10.3390/ijms18102142.

(16) Neves, M. A.; Reinstein, O.; Johnson, P. E. Defining a Stem Length-Dependent Binding Mechanism for the Cocaine-Binding Aptamer. A Combined NMR and Calorimetry Study. *Biochemistry* **2010**, *49* (39), 8478–8487.

(17) Lin, C. H.; Patei, D. J. Structural Basis of DNA Folding and Recognition in an AMP-DNA Aptamer Complex: Distinct Architectures but Common Recognition Motifs for DNA and RNA Aptamers Complexed to AMP. *Chem. Biol.* **1997**, *4* (11), 817–832. https://doi.org/10.1016/S1074-5521(97)90115-0.

(18) Xu, G.; Zhao, J.; Yu, H.; Wang, C.; Huang, Y.; Zhao, Q.; Zhou, X.; Li, C.; Liu, M. Structural Insights into the Mechanism of High-Affinity Binding of Ochratoxin A by a DNA Aptamer. *J. Am. Chem. Soc.* **2022**, *144* (17), 7731–7740. https://doi.org/10.1021/jacs.2c00478.

(19) Dolot, R.; Lam, C. H.; Sierant, M.; Zhao, Q.; Liu, F.-W.; Nawrot, B.; Egli, M.; Yang, X. Crystal Structures of Thrombin in Complex with Chemically Modified Thrombin DNA Aptamers Reveal the Origins of Enhanced Affinity. *Nucleic Acids Res.* **2018**, *46* (9), 4819–4830. https://doi.org/10.1093/nar/gky268.

(20) Slavkovic, S.; Zhu, Y.; Churcher, Z. R.; Shoara, A. A.; Johnson, A. E.; Johnson, P. E. Thermodynamic Analysis of Cooperative Ligand Binding by the ATP-Binding DNA Aptamer Indicates a Population-Shift Binding Mechanism. *Sci. Rep.* **2020**, *10* (1), 18944. https://doi.org/10.1038/s41598-020-76002-8.

(21) Neves, M. A.; Slavkovic, S.; Churcher, Z. R.; Johnson, P. E. Salt-Mediated Two-Site Ligand Binding by the Cocaine-Binding Aptamer. *Nucleic Acids Res.* **2017**, *45* (3), 1041–1048. https://doi.org/10.1093/nar/gkw1294.

(22) Tesmer, J. J. Crystallographic Pursuit of a Protein-RNA Aptamer Complex. *Methods Mol. Biol. (N. Y., NY, U. S.)* **2016**, 151–160. https://doi.org/10.1007/978-1-4939-3197-2_12.

(23) Lebars, I.; Legrand, P.; Aimé, A.; Pinaud, N.; Fribourg, S.; Di Primo, C. Exploring TAR–RNA Aptamer Loop–Loop Interaction by X-Ray Crystallography, UV Spectroscopy and Surface Plasmon Resonance. *Nucleic Acids Res.* **2008**, *36* (22), 7146–7156. https://doi.org/10.1093/nar/gkn831.

(24) Ruigrok, V. J.; Levisson, M.; Hekelaar, J.; Smidt, H.; Dijkstra, B. W.; Van der Oost, J. Characterization of Aptamer-Protein Complexes by X-Ray Crystallography and Alternative Approaches. *Int. J. Mol. Sci.* **2012**, *13* (8), 10537–10552. https://doi.org/10.3390/ijms130810537.

(25) Ahmad, N. A.; Mohamed Zulkifli, R.; Hussin, H.; Nadri, M. H. In Silico Approach for Post-SELEX DNA Aptamers: A Mini-Review. *J. Mol. Graphics Modell.* **2021**, *105*, 107872. https://doi.org/10.1016/j.jmgm.2021.107872.

(26) Wu, Y.; Ranallo, S.; Del Grosso, E.; Chamoro-Garcia, A.; Ennis, H. L.; Milosavić, N.; Yang, K.; Kippin, T.; Ricci, F.; Stojanovic, M. Using Spectroscopy to Guide the Adaptation of Aptamers into Electrochemical Aptamer-Based Sensors. *Bioconjugate Chem.* **2022**. https://doi.org/10.1021/acs.bioconjchem.2c00275.

(27) Xiao, Y.; Uzawa, T.; White, R. J.; DeMartini, D.; Plaxco, K. W. On the Signaling of Electrochemical Aptamer-Based Sensors: Collision-and Folding-Based Mechanisms. *Electroanalysis* **2009**, *21* (11), 1267–1271. https://doi.org/10.1002/elan.200804564.

(28) Ricci, F.; Plaxco, K. W. E-DNA Sensors for Convenient, Label-Free Electrochemical Detection of Hybridization. *Microchim. Acta* **2008**, *163*, 149–155. https://doi.org/10.1007/s00604-008-0015-4.

(29) White, R. J.; Phares, N.; Lubin, A. A.; Xiao, Y.; Plaxco, K. W. Optimization of Electrochemical Aptamer-Based Sensors via Optimization of Probe Packing Density and Surface Chemistry. *Langmuir* **2008**, *24* (18), 10513–10518. https://doi.org/10.1021/la800801v.

(30) Chinnappan, R.; AlZabn, R.; Abu-Salah, K. M.; Zourob, M. An Aptamer Based Fluorometric Microcystin-LR Assay Using DNA Strand-Based Competitive Displacement. *Microchim. Acta* **2019**, *186* (7), 1–10. https://doi.org/10.1007/s00604-019-3504-8.

(31) Gold, L.; Polisky, B.; Uhlenbeck, O.; Yarus, M. Diversity of Oligonucleotide Functions. *Annu. Rev. Biochem.* **1995**, *64* (1), 763–797. https://doi.org/doi: 10.1146/annurev.bi.64.070195.003555.

(32) Fadock, K. L.; Manderville, R. A. DNA Aptamer–Target Binding Motif Revealed Using a Fluorescent Guanine Probe: Implications for Food Toxin Detection. *ACS Omega* **2017**, *2* (8), 4955–4963. https://doi.org/10.1021/acsomega.7b00782.

(33) Neves, M. A.; Reinstein, O.; Saad, M.; Johnson, P. E. Defining the Secondary Structural Requirements of a Cocaine-Binding Aptamer by a Thermodynamic and Mutation Study. *Biophys. Chem.* **2010**, *153* (1), 9–16. https://doi.org/10.1016/j.bpc.2010.09.009.

(34) Mieczkowski, M.; Steinmetzger, C.; Bessi, I.; Lenz, A.-K.; Schmiedel, A.; Holzapfel, M.; Lambert, C.; Pena, V.; Höbartner, C. Large Stokes Shift Fluorescence Activation in an RNA Aptamer by Intermolecular Proton Transfer to Guanine. *Nat. Commun.* **2021**, *12* (1), 3549. https://doi.org/10.1038/s41467-021-23932-0.

(35) Padmanabhan, K.; Padmanabhan, K. P.; Ferrara, J. D.; Sadler, J. E.; Tulinsky, A. The Structure of Alpha-Thrombin Inhibited by a 15-Mer Single-Stranded DNA Aptamer. *J. Biol. Chem.* **1993**, *268* (24), 17651–17654. https://doi.org/doi: 10.2210/pdb1hut/pdb.

(36) Tsiang, M.; Gibbs, C. S.; Griffin, L. C.; Dunn, K. E.; Leung, L. L. Selection of a Suppressor Mutation That Restores Affinity of an Oligonucleotide Inhibitor for Thrombin Using in Vitro Genetics. *J. Biol. Chem.* **1995**, *270* (33), 19370–19376. https://doi.org/doi: 10.1074/jbc.270.33.19370.

(37) Park, S.; Jeong, J.-E.; Le, V. S.; Seo, J.; Yu, B.; Kim, D.-Y.; Kwon, S.-H.; Jon, S.; Woo, H. Y.; Yang, H. Enhanced Electron Transfer Mediated by Conjugated Polyelectrolyte and Its Application to Washing-Free DNA Detection. *J. Am. Chem. Soc.* **2018**, *140* (7), 2409–2412. https://doi.org/10.1021/jacs.7b12382.

(38) Chazalviel, J.-N.; Allongue, P. On the origin of the efficient nanoparticle mediated electron transfer across a self-assembled monolayer. *Journal of the American Chemical Society* **2011**, *133* (4), 762–764. https://doi.org/10.1021/ja109295x.

(39) Lee, H.; Chang, B.-Y.; Kwack, W.-S.; Jo, K.; Jeong, J.; Kwon, S.-H.; Yang, H. Dependence of the Capacitance between an Electrode and an Electrolyte Solution on the Thickness of Aluminum Oxide Layers Deposited Using Atomic Layer Deposition. *J. Electroanal. Chem.* **2013**, *700*, 8–11. https://doi.org/10.1016/j.jelechem.2013.04.008.

(40) He, J.; Wang, J.; Zhang, M.; Shi, G. Selection of a Structure-Switching Aptamer for the Specific Methotrexate Detection. *ACS Sens.* **2021**, *6* (6), 2436–2441. https://doi.org/10.1021/acssensors.1c00749.

(41) Shaver, A.; Mahlum, J. D.; Scida, K.; Johnston, M. L.; Aller Pellitero, M.; Wu, Y.; Carr, G. V.; Arroyo-Currás, N. Optimization of Vancomycin Aptamer Sequence Length Increases the Sensitivity of Electrochemical, Aptamer-Based Sensors In Vivo. *ACS Sens.* **2022**, *7* (12), 3895–3905. https://doi.org/10.1021/acssensors.2c01910.

(42) Alkhamis, O.; Canoura, J.; Ly, P. T.; Xiao, Y. Using Exonucleases for Aptamer Characterization, Engineering, and Sensing. *Acc. Chem. Res.* **2023**, *56* (13), 1731–1743. https://doi.org/10.1021/acs.accounts.3c00113.

(43) Canoura, J.; Wang, Z.; Yu, H.; Alkhamis, O.; Fu, F.; Xiao, Y. No Structure-Switching Required: A Generalizable Exonuclease-Mediated Aptamer-Based Assay for Small-Molecule Detection. *J. Am. Chem. Soc.* **2018**, *140* (31), 9961–9971. https://doi.org/10.1021/jacs.8b04975.

(44) Wang, Z.; Yu, H.; Canoura, J.; Liu, Y.; Alkhamis, O.; Fu, F.; Xiao, Y. Introducing Structure-Switching Functionality into Small-Molecule-Binding Aptamers via Nuclease-Directed Truncation. *Nucleic Acids Res.* **2018**, *46* (13), e81–e81.

(45) Nakatsuka, N.; Yang, K.-A.; Abendroth, J. M.; Cheung, K. M.; Xu, X.; Yang, H.; Zhao, C.; Zhu, B.; Rim, Y. S.; Yang, Y.; Weiss, P. S.; Stojanović, M. N.; Andrews, A. M. Aptamer-Field-Effect Transistors Overcome Debye Length Limitations for Small-Molecule Sensing. *Science* **2018**, *362* (6412), 319–324. https://doi.org/10.1126/science.aao6750.

(46) Huang, P.-J. J.; Liu, J. A DNA Aptamer for Theophylline with Ultrahigh Selectivity Reminiscent of the Classic RNA Aptamer. *ACS Chem. Biol.* **2022**, *17* (8), 2121–2129. https://doi.org/10.1021/acschembio.2c00179.

(47) White, R. J.; Rowe, A. A.; Plaxco, K. W. Re-Engineering Aptamers to Support Reagentless, Self-Reporting Electrochemical Sensors. *Analyst* **2010**, *135* (3), 589–594. https://doi.org/10.1039/b921253a.

(48) Xiao, Y.; Lai, R. Y.; Plaxco, K. W. Preparation of Electrode-Immobilized, Redox-Modified Oligonucleotides for Electrochemical DNA and Aptamer-Based Sensing. *Nat. Protoc.* **2007**, *2* (11), 2875–2880. https://doi.org/10.1038/nprot.2007.413.

(49) Rahbarimehr, E.; Chao, H. P.; Churcher, Z. R.; Slavkovic, S.; Kaiyum, Y. A.; Johnson, P. E.; Dauphin-Ducharme, P. Finding the Lost Dissociation Constant of Electrochemical Aptamer-Based Biosensors. *Anal. Chem.* **2023**, *95* (4), 2229–2237. https://doi.org/10.1021/acs.analchem.2c03566.

(50) Fontaine, N.; Dauphin-Ducharme, P. Confounding Effects on the Response of Electrochemical Aptamer-Based Biosensors. *Curr. Opin. Electrochem.* **2023**, 101361. https://doi.org/10.1016/j.coelec.2023.101361.

(51) Neves, M. A. D.; Shoara, A. A.; Reinstein, O.; Abbasi Borhani, O.; Martin, T. R.; Johnson, P. E. Optimizing Stem Length To Improve Ligand Selectivity in a Structure-Switching Cocaine-Binding Aptamer. *ACS Sens.* **2017**, *2* (10), 1539–1545. https://doi.org/10.1021/acssensors.7b00619.

(52) Lu, C.; Jimmy Huang, P.-J.; Zheng, J.; Liu, J. 2-Aminopurine Fluorescence Spectroscopy for Probing a Glucose Binding Aptamer. *ChemBioChem* **2022**, *23* (12), e202200127. https://doi.org/10.1002/cbic.202200127.

(53) Pearce, R.; Omenn, G. S.; Zhang, Y. De Novo RNA Tertiary Structure Prediction at Atomic Resolution Using Geometric Potentials from Deep Learning. *bioRxiv* **2022**, 2022.05. 15.491755. https://doi.org/10.1101/2022.05.15.491755.

(54) Lu, X.-J.; Olson, W. K. 3DNA: A Software Package for the Analysis, Rebuilding and Visualization of Three-dimensional Nucleic Acid Structures. *Nucleic Acids Res.* **2003**, *31* (17), 5108–5121. https://doi.org/10.1093/nar/gkg680.

(55) Schrodinger, L. The PyMOL Molecular Graphics System, Version 1.3r1., 2010.

(56) Vilar, S.; Cozza, G.; Moro, S. Medicinal Chemistry and the Molecular Operating Environment (MOE): Application of QSAR and Molecular Docking to Drug Discovery. *Curr. Top. Med. Chem.* **2008**, *8* (18), 1555–1572. https://doi.org/10.2174/156802608786786624.

(57) Eberhardt, J.; Santos-Martins, D.; Tillack, A. F.; Forli, S. AutoDock Vina 1.2.0: New Docking Methods, Expanded Force Field, and Python Bindings. *J. Chem. Inf. Model.* **2021**, *61* (8), 3891–3898. https://doi.org/10.1021/acs.jcim.1c00203.

(58) Biovia, D. S. Dassault Systèmes. *San Diego* **2017**.

(59) Wolfe, M.; Cramer, A.; Webb, S.; Goorskey, E.; Chushak, Y.; Mirau, P.; Arroyo-Currás, N.; Chávez, J. L. Rational Approach to Optimizing Conformation-Switching Aptamers for Biosensing Applications. *ACS Sens.* **2024**, *9* (2), 717–725. https://doi.org/10.1021/acssensors.3c02004.

(60) Yu, Y.; Chen, K.; Du, Z.; Fang, B.; Zhan, J.; Zhu, L.; Xu, W. Magnetic Aptamer Copper Nanoclusters Fluorescent Biosensor for the Visual Detection of Zearalenone Based on Docking-Aided Rational Tailoring. *Food Chemistry* **2024**, 139127. https://doi.org/10.1016/j.foodchem.2024.139127.

(61) Liang, G.; Zhao, J.; Gao, Y.; Xie, T.; Zhen, J.; Pan, L.; Gong, W. Application and Evaluation of Molecular Docking for Aptamer and Small Molecular Interaction-A Case Study with Tetracycline Antibiotics. *Talanta* **2024**, *266*, 124942. https://doi.org/10.1016/j.talanta.2023.124942.

(62) Chen, K.; Zhu, L.; Du, Z.; Lan, X.; Huang, K.; Zhang, W.; Xu, W. Docking-Aided Rational Tailoring of a Fluorescence-and Affinity-Enhancing Aptamer for a Label-Free Ratiometric Malachite Green Point-of-Care Aptasensor. *J. Hazard. Mater.* **2023**, *447*, 130798. https://doi.org/10.1016/j.jhazmat.2023.130798.

(63) Guan, Y.; Ma, J.; Neng, J.; Yang, B.; Wang, Y.; Xing, F. A Novel and Label-Free Chemiluminescence Detection of Zearalenone Based on a Truncated Aptamer Conjugated with a G-Quadruplex DNAzyme. *Biosensors* **2023**, *13* (1), 118. https://doi.org/10.3390/bios13010118.

(64) Navien, T. N.; Thevendran, R.; Hamdani, H. Y.; Tang, T.-H.; Citartan, M. In Silico Molecular Docking in DNA Aptamer Development. *Biochimie* **2021**, *180*, 54–67. https://doi.org/10.1016/j.biochi.2020.10.005.

(65) Baba, N.; Akaho, E. VSDK: Virtual Screening of Small Molecules Using AutoDock Vina on Windows Platform. *Bioinformation* **2011**, *6* (10), 387. https://doi.org/doi: 10.6026/97320630006387.

(66) Forli, S.; Huey, R.; Pique, M. E.; Sanner, M. F.; Goodsell, D. S.; Olson, A. J. Computational Protein–Ligand Docking and Virtual Drug Screening with the AutoDock Suite. *Nat. Protoc.* **2016**, *11* (5), 905–919. https://doi.org/10.1038/nprot.2016.051.

(67) Tessaro, F.; Scapozza, L. How 'Protein-Docking'Translates into the New Emerging Field of Docking Small Molecules to Nucleic Acids? *Molecules* **2020**, *25* (12), 2749. https://doi.org/10.3390/molecules25122749.

(68) Pagadala, N. S.; Syed, K.; Tuszynski, J. Software for Molecular Docking: A Review. *Biophys. Rev.* **2017**, *9*, 91–102. https://doi.org/doi: 10.1007/s12551-016-0247-1.

(69) Taghizadeh, M. S.; Niazi, A.; Moghadam, A.; Afsharifar, A. Experimental, Molecular Docking and Molecular Dynamic Studies of Natural Products Targeting Overexpressed Receptors in Breast Cancer. *PLoS One* **2022**, *17* (5), e0267961. https://doi.org/doi: 10.1371/journal.pone.0267961.

(70) Huey, R.; Morris, G. M.; Forli, S. *Using AutoDock 4 and AutoDock Vina with AutoDockTools: A Tutorial*. The Scripps Research Institute Molecular Graphics Laboratory.

(71) Trott, O.; Olson, A. J. AutoDock Vina: Improving the Speed and Accuracy of Docking with a New Scoring Function, Efficient Optimization, and Multithreading. *J. Comput. Chem.* **2010**, *31* (2), 455–461. https://doi.org/10.1002/jcc.21334.

(72) Bursulaya, B. D.; Totrov, M.; Abagyan, R.; Brooks, C. L. Comparative Study of Several Algorithms for Flexible Ligand Docking. *J. Comput.-Aided Mol. Des.* **2003**, *17*, 755–763. https://doi.org/doi: 10.1023/b:jcam.0000017496.76572.6f.

(73) Ben Aissa, S.; Mastouri, M.; Catanante, G.; Raouafi, N.; Marty, J. L. Investigation of a Truncated Aptamer for Ofloxacin Detection Using a Rapid FRET-Based Apta-Assay. *Antibiotics* **2020**, *9* (12), 860. https://doi.org/doi: 10.3390/antibiotics9120860.

(74) Rodríguez Serrano, A. F.; Hsing, I.-M. Prediction of Aptamer–Small-Molecule Interactions Using Metastable States from Multiple Independent Molecular Dynamics Simulations. *J. Chem. Inf. Model.* **2022**, *62* (19), 4799–4809. https://doi.org/10.1021/acs.jcim.2c00734.

(75) Buglak, A. A.; Samokhvalov, A. V.; Zherdev, A. V.; Dzantiev, B. B. Methods and Applications of In Silico Aptamer Design and Modeling. *Int. J. Mol. Sci.* **2020**, *21* (22), 8420. https://doi.org/10.3390/ijms21228420.

(76) Sharma, S.; Kumar, P.; Chandra, R. *Applications of BIOVIA Materials Studio, LAMMPS, and GROMACS in Various Fields of Science and Engineering*; Elsevier B.V., 2019.

(77) Adachi, T.; Nakamura, Y. Aptamers: A Review of Their Chemical Properties and Modifications for Therapeutic Application. *Molecules* **2019**, *24* (23), 4229. https://doi.org/doi: 10.3390/molecules24234229.

(78) Xie, Y.; Wu, S.; Chen, Z.; Jiang, J.; Sun, J. Rapid Nanomolar Detection of Methamphetamine in Biofluids via a Reagentless Electrochemical Aptamer-Based Biosensor. *Anal. Chim. Acta* **2022**, *1207*, 339742. https://doi.org/10.1016/j.aca.2022.339742.

(79) Dauphin Ducharme, P.; Churcher, Z. R.; Shoara, A. A.; Rahbarimehr, E.; Slavkovic, S.; Fontaine, N.; Boisvert, O.; Johnson, P. E. Redox Reporter–Ligand Competition to Support Signaling in the Cocaine-binding Electrochemical Aptamer-based Biosensor. *Chem. - Eur. J.* e202300618. https://doi.org/10.1002/chem.202300618.

(80) Li, D.; Song, S.; Fan, C. Target-Responsive Structural Switching for Nucleic Acid-Based Sensors. *Acc. Chem. Res.* **2010**, *43* (5), 631–641. https://doi.org/10.1021/ar900245u.

(81) Albrecht, T. Electrochemical Tunnelling Sensors and Their Potential Applications. *Nat. Commun.* **2012**, *3* (1), 829. https://doi.org/10.1038/ncomms1791.

(82) Shoichet, B. K.; Leach, A. R.; Kuntz, I. D. Ligand Solvation in Molecular Docking. *Proteins: Struct., Funct., Bioinf.* **1999**, *34* (1), 4–16. https://doi.org/10.1002/(SICI)1097-0134(19990101)34:1<4::AID-PROT2>3.0.CO;2-6.

(83) Hollingsworth, S. A.; Dror, R. O. Molecular Dynamics Simulation for All. *Neuron* **2018**, *99* (6), 1129–1143. https://doi.org/10.1016/j.neuron.2018.08.011.

(84) Lee, S. J.; Cho, J.; Lee, B.-H.; Hwang, D.; Park, J.-W. Design and Prediction of Aptamers Assisted by In Silico Methods. *Biomedicines* **2023**, *11* (2), 356. https://doi.org/10.3390/biomedicines11020356.

602 **For TOC only**

603

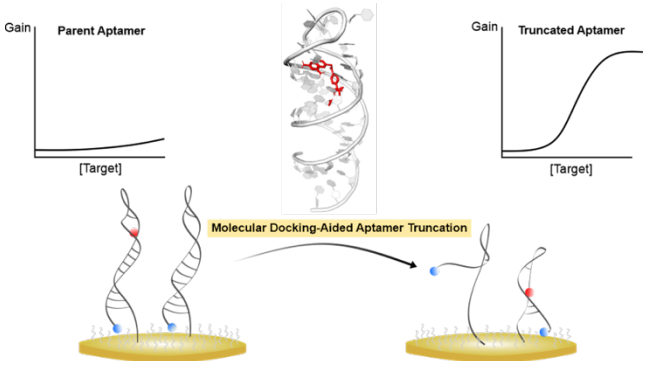

604